

Segmentation of Moiré Fringes of Scoliotic Spines Using Filtering and Morphological Operations

**Csaba Bogdán¹, Andor Dániel Magony¹, Wolfgang Birkfellner²,
Ákos Antal³, Miklós Tunyogi-Csapó⁴**

¹ Institute of Transdisciplinary Discoveries, Medical School, University of Pécs, Ifjúság útja 11, H-7624 Pécs, Hungary; csaba.bogdan@pte.hu; magony.andor@pte.hu

² Center for Medical Physics and Biomedical Engineering, Medical University of Vienna Spitalgasse 23, A-1090 Vienna, Austria; wolfgang.birkfellner@meduniwien.ac.at

³ Department of Mechatronics, Optics and Mechanical Engineering Informatics, Budapest University of Technology and Economics, Bertalan Lajos u. 4-6, H-1111, Budapest, Hungary; akos@mogi.bme.hu

⁴ National Center for Spinal Disorders, Buda Health Center, Királyhágó u. 1-3, H-1126 Budapest, Hungary; miklos.tunyogi@bhc.hu

Abstract: For reducing uncertainties in moiré pattern analysis, an accurate segmentation of moiré fringes (MF) is vital. In this study, an algorithm for segmenting MFs of scoliotic spines was provided in MATLAB® environment by an empirically established sequence of filtering and morphological operations defined by static function parameters: (1) contrast enhancement, (2) brightness increase, (3) contrast refinement, (4) 2-D Gaussian filter, (5) dilation, (6) thresholding, (7) skeletonization. The algorithm is simple, fast to process and, for the most part of the images, follows the MFs correctly. Further research on segmenting MFs is quite promising by improving the algorithm with adaptive and dynamic solutions, and exploring ways to replace time demanding and complex image processing techniques.

Keywords: moiré fringe segmentation; moiré method; shadow moiré; projection moiré; digital moiré; scoliosis

1 Introduction

Diagnosing spinal deformities has long been in the focus of medicine. Measurement of bending disorders of the vertebral column, such as scoliosis, is usually performed on radiographs by calculating the Cobb angle. Disadvantages of

X-ray imaging such as cost, time and repetition demands, tools and environmental conditions required and radiation exposure imparted to the patient, are not negligible, and justify methodological research of such moiré technique or moiré topography, that can lead to fast, cost-effective and non-ionizing diagnostic imaging of the spine.

The phenomenon of moiré [mwaké] or moiré effect was elevated to scientific status, first, by Lord Rayleigh dealing with diffraction gratings in 1874 [1]. Lord Rayleigh concluded that moiré might be made useful for measurement purposes. About 100 years later, beyond industrial applications, further research proposed moiré topography for measurement of the human body [2], [3]. From the 1980s, MT is used on the whole human body, including oral cavity [4], bones [5], teeth and the skeletal system [6].

Moiré refers to an irregular wavy surface the pattern of which changes in accordance with its movement and can be observed, if two or more structures with similar geometry (nearly identical arrays of lines or dots) overlap, producing alternating bright and dark fringes (Fig. 1). Usually, dark fringes are called moiré fringes (MFs) or moiré stripes, but we can also consider bright ones as moiré surfaces when examining moiré images (MIs)—it is only a matter of agreement [7]. Based on the physical phenomenon of moiré, moiré techniques are defined as a group of methods usually used for surface mapping and shape or deformation measurement. In the scientific literature, shadow moiré and projection moiré techniques (SMT and PMT, respectively) seem to be the two primary methods of MT used for measurement of the human body (Fig. 2-3) [8].

An algorithm based on MT that proved to be suitable for calculating the curvature angle of the spine, may complement or substitute X-ray images—especially in follow-up examinations. The workload required for segmentation and evaluation of MIs is, however, not inconsiderable; some researchers see the best solution for that in an automatic system [8], [9], [10], [11], [12], [13]. And yet, processing of MIs requires several unique solutions that are especially influenced by optical arrangement, applied illumination (effect on intensity distribution), nature of noise and detection. Therefore, implementing a fully automated image analysis is a challenging, nevertheless desired objective in the field [7], [14]. For reducing uncertainties in moiré pattern analysis, an accurate segmentation of MFs is vital. The present study aims to contribute to the segmenting phase of MI analysis of scoliotic spines by providing an algorithm of filtering and morphological operations. This study presents the initial phase of the research, where static function parameters were applied to identify a possible segmenting sequence for MFs. Segmentation with adaptive and dynamic function parameters is not the subject of the present study but can be expected in a later phase of the research.

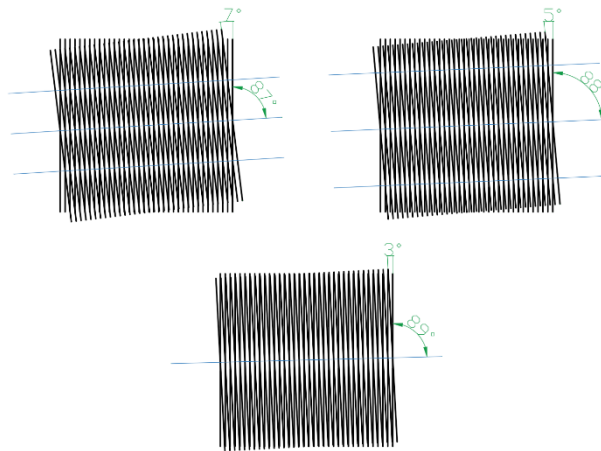


Figure 1

Moiré fringes of identical grids with different angle deviations

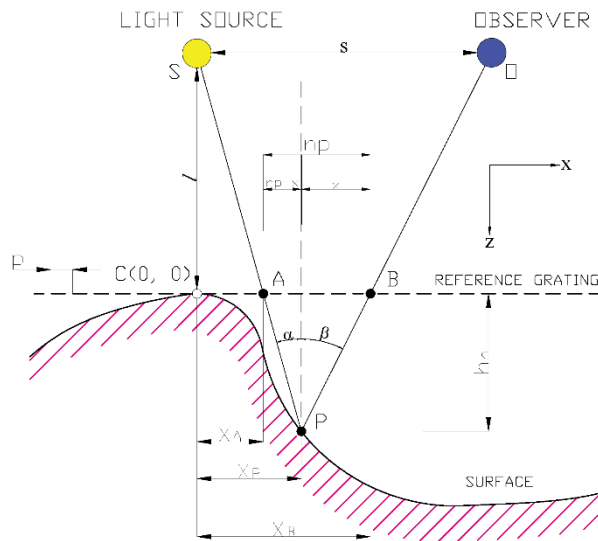


Figure 2

The base principle of shadow moiré technique

- (A) Point where source light S passes through the reference grating
- (B) Point where reflected source light S passes through the reference grating
- (C) Origin
- (O) Observer
- (p) Grating pitch (or period of the grating)
- (P) Measured point
- (S) Light source

- (α) Incidence angle (of incoming light)
- (β) Viewing angle
- (h_n) Depth of n^{th} -order moiré pattern measured from the reference grating
- (l) Distance of S and O from the reference grating surface
- (n) Order of the moiré pattern
- (s) Interseparation of S and O
- (X_A) X component of SA distance
- (X_B) X component of SB distance
- (X_P) X component of SP distance
- (x) X component of PB distance

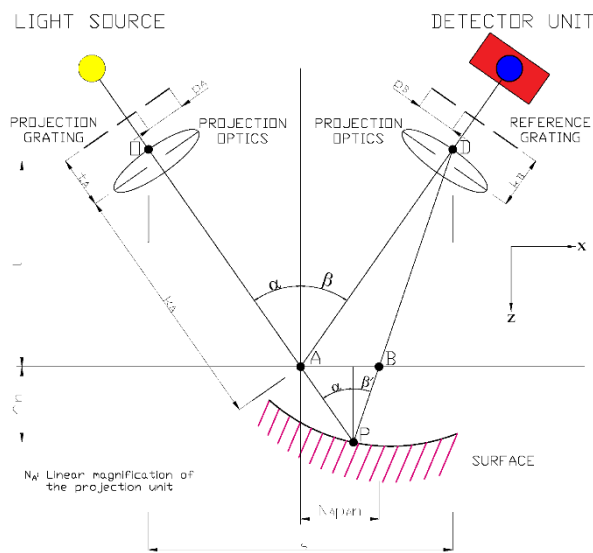


Figure 3

The base principle of projection moiré technique

- (A) Point where source light passes through the reference plane
- (B) Point where reflected source light passes through the reference plane
- (D) Projection optics on the detector's side
- (h_n) Depth of n^{th} -order moiré pattern measured from the reference plane
- (k_A) Distance between A and projection optics on the illumination's side
- (k_B) Distance between the reference grating and optics on the detector's side
- (l) Distance of projection and reference grating measured from the reference plane
- (n) Order of the moiré pattern
- (N_A) Linear magnification of the projection unit
- (O) Projection optics
- (P) Measured point
- (p_A) Pitch of projection grating

- (p_B) Pitch of reference grating
- (s) Distance between the projection optics O and D
- (t_A) Distance between the projection grating and optics on the illumination's side
- (α) Incidence angle (of incoming light)
- (β) Viewing angle at A
- (β') Viewing angle at P

2 Materials and Methods

The segmenting algorithm was developed in MATLAB[®] version 9.5.0.944444 (R2018b) [15] based on exploratory sequences and observations performed on 11 MIs made available by SALUS Ortopédtechnika Kft. Original MIs were software-generated applying digital PMT, and have a resolution of 2448 x 3264 px in 10 cases and 2736 x 3648 px in 1 single case with a bit depth of 24 and DPI of 96. MIs show patients in standing position facing the reference wall, and non-ROI areas that typically contain irrelevant image content of residual grating and non-moiré parts outside the back region. The procedure of image processing involves two main phases: (1) preprocessing MIs, (2) segmenting MFs using a sequence of filtering and morphological operations. Based on operation parameters applied in phase (2), two MI groups (G1, G2) are distinguished. For MIs in G1, identical parameters of processing phases result the similar outcome. For G2, different parameters are required for similar results, even in the group itself (Table 1). The reason for this is to be found in different image characteristics in terms of contrast, noise and moiré blur/confluence that are likely to result from dissimilar measurement setups. The phases of the code are illustrated in MI no. 2 of G1 (Fig. 4-14). For the other images, only the result of the segmentation is given in the overlap with grayscale ROIs (Fig. 15-20).

2.1 Preprocessing Moiré Images

In the first phase of image processing, original MIs are prepared for further processing by (a) manual selection of region of interests (ROIs) and (b) conversion into grayscale. As a result of these steps, input images for phase 2 are obtained. Selection of ROIs is performed by rectangular cropping using *imcrop* function. Original images are reduced in size based on selected ROI area with boundaries from the neck to the hip; and from the left upper arm to the right one (Fig. 4). Cropped images vary in size according to the size of specific ROI area and patient setup (distance from the camera). The resolutions of cropped images are between the range of 784x1044 px and 1136x1406 px.



Figure 4
Original (L) and ROI-cropped (R) moiré image

Function *rgb2gray* is applied in order to convert cropped RGB images into grayscale (Fig. 5). For morphological operations discussed in phase (2), grayscale images contain all the relevant information of moiré stripes. Colour intensity values do not carry additional information here, and their conversion to grayscale does not induce data loss.

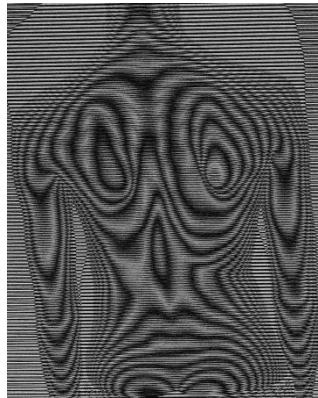


Figure 5
Grayscale moiré image with ROI

2.2 Steps of Moiré Fringe Segmentation

For segmenting MFs, a possible algorithmic approach is introduced. In the segmentation procedure, an empirically established sequence of filtering and morphological operations is used: (1) enhancing contrast, (2) increasing brightness, (3) refining contrast, applying (4) 2-D Gaussian filter and (5) dilation, (6) thresholding and (7) skeletonization.

Table 1
Summary of function parameters applied to moiré image (MI) groups G1 and G2

Phases	G1 (MI no. 1, 2, 3, 5, 6, 7, 9, 10)	G2 (MI no. 4, 8, 11)
Enhancing contrast [<i>imadjust</i> by def.]	3x	3x
Increasing brightness [increase in pixel value]	120	100 for MI no. 4 and 8 110 for MI no. 11
Refining contrast [range of intensity values]	[0.7 1]	[0.7 1]
2-D Gaussian filter [standard deviation]	6	6 for MI no. 4 and 11 8 for MI no. 8
Dilation [structuring element, pixel width, repetition]	square, 3, 3	square, 3, 3
Threshold value	0.41	0.35 for MI no. 4 and 11 0.38 for MI no. 8

2.2.1 Enhancing Contrast

For mapping the intensity values to new values and thereby enhancing contrast, *imadjust* function was applied in 2 steps. In the first step a slight contrast correction is performed via saturating the bottom 1% and the top 1% of all pixel values three times by the default operation of *imadjust* (Fig. 6).

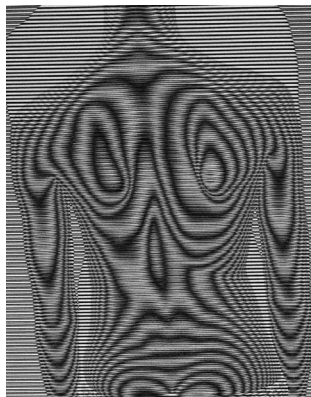


Figure 6

Result of contrast enhancement applied on grayscale moiré

2.2.2 Increasing Brightness

Before further contrast enhancement, brightness is increased by increasing pixel values of MIs of G1 by 120 and G2 by 100 and 110, respectively (Fig. 7).

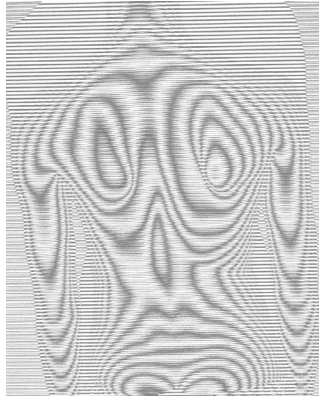


Figure 7
Result of brightness increase

2.2.3 Refining Contrast

As the second step in contrast adjustment, intensity values are mapped to new values between 0.7 and 1, by re-applying the function *imadjust*. The result is a stronger contrast of moiré stripes (Fig. 8).

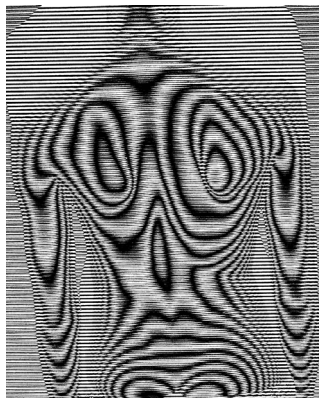


Figure 8
Result of contrast refinement

2.2.4 Applying 2-D Gaussian Filter

Image is filtered with a 2-D Gaussian smoothing kernel (*imgaussfilt*) with image specific standard deviation values 6 or 8 (Fig. 9).

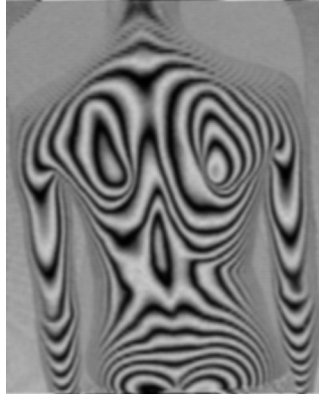


Figure 9
Result of 2-D Gaussian filtering

2.2.5 Applying Dilation

Blurred grayscale image is dilated by using *imdilate* and morphological structuring element *strel*. Dilation is applied three times in combination of square structuring element with a width of 3 pixels (Fig. 10). In Fig. 10, resulting differences from the previous step (2-D Gaussian filter) may not be obvious, however, dilation supports the results of thresholding and skeletonizing operations by gradually enlarging the boundaries of regions of foreground pixels.

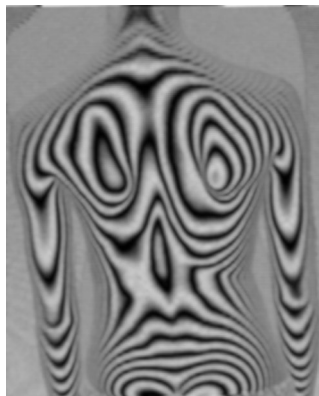


Figure 10
Result of dilation

2.2.6 Thresholding

Function *imbinarize* is used to convert the image to a binary image, based on a threshold value: all pixel values above a globally determined threshold are replaced with ones and all other values with zeros. The threshold value applied is covered in the range between 0.35 and 0.41 (Fig. 11).



Figurer 11
Result of thresholding

2.2.7 Skeletonization

Skeletonization was performed by using *bwmorph* function for morphological operations, specified as 'thin'. The operation 'thin' is applied for thinning binarized images to single lines, and repeated until the image no longer changes (i.e. parameter 'Inf' in the function input). The inputs of *bwmorph* are provided by complements of binarized images generated with the function *imcomplement*. For a better visualization of the results, lines of skeletonized images are fattened by applying the operation 'fatten' once. The result is shown enlarged as re-complemented image (Fig. 12) and as overlay on binarized (Fig. 13) and colour ROI images (Fig. 14).



Figure 12

Result of skeletonization: segmented moiré fringes



Figure 13

Overlay of segmented moiré fringes (green) on thresholded image (black)



Figure 14

Overlay of segmented moiré fringes on colour ROI

3 Results and Discussion

Results show that the segmenting method is simple, fast to process and, for the most part of the image, follows the moiré stripes accurately (Fig 15-20). The average processing time of the algorithm from grayscale conversion to skeletonization is 0.146 s per image. In Table 2, the time course of the algorithm, with exclusion of manual ROI selection, is summarized in average elapsed and processing time.

The segmenting algorithm leads to a partial or sporadic segmentation of moiré stripes. Image details (i.e. parts of moiré stripes) and accuracy are lost mainly due to original fringe quality and characteristics such as (a) pale—mostly around the shoulders and the waist—, (b) convergent, (c) wider/blurred MFs, (d) image noise caused mostly by residual grating, and (e) unwanted branches generated by skeletonizing operation (Fig. 21). In terms of general usability of the code, the

necessity of re-adjusting static function parameters is challenging and—especially in higher patient populations—time consuming. To get similar results on MIs other than the 11 sample images applied in this study, function parameters need to be empirically determined and implemented in the code. Therefore, static function parameters are desired to be eliminated with automatic adaptive and dynamic parameterization. Also, for problems (a-e), a more sensible solution is required. A possible way for further research might be to improve the algorithm with (1) adaptive and dynamic function parameters based on values of low contrasted and over contrasted images in combination with adaptive thresholds, (2) applying high-pass filters for image sharpening. Another possible direction of research is (3) to combine the algorithm with segmentation approaches based on a fuzzy inference system [16]. Due to its simplicity and fast operation, an improved solution of the algorithm could also replace time demanding and complex segmentation methods.

Table 2
Time course of the segmenting algorithm

Proc. Nr.	Process	Average Time [sec]*	
		<i>Elapsed</i>	<i>Processing</i>
1	Manual selection of ROI	excl.	excl.
2	Determining object class	0.02567	0.02567
3	Duplicating image for reference	0.02593	0.00026
4	Converting in grayscale	0.02717	0.00124
5	Enhancing contrast	0.03990	0.01272
6	Increasing brightness	0.04036	0.00046
7	Refining contrast	0.04348	0.00312
8	2-D Gaussian filter	0.05781	0.01433
9	Dilation	0.06195	0.00414
10	Thresholding	0.06901	0.00705
11	Skeletonization	0.17165	0.10264
12	Saving images in <i>.png</i> files*	0.61555	0.44390
13	Visualizing results	0.73376	0.11821

*System used: CPU: Intel® Core™ i5-8300H @ 2.30 GHz,
GPU: NVIDIA GeForce GTX 1050 (4 GB), RAM: 8 GB

**Output images are saved as skeletonized moiré contours
(transparent and white-backgrounded) and its overlays on
binarized and input images.

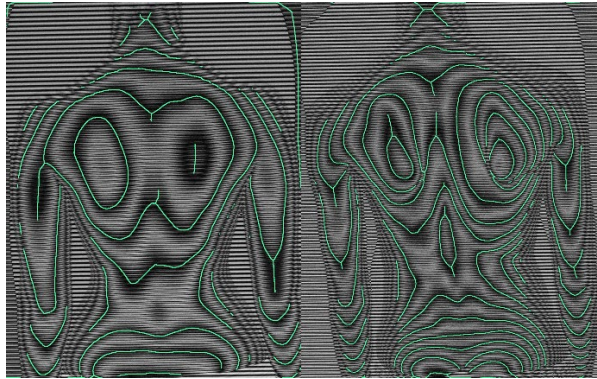


Figure 15
Segmented moiré fringes of image no. 1 (L) and 2 (R)

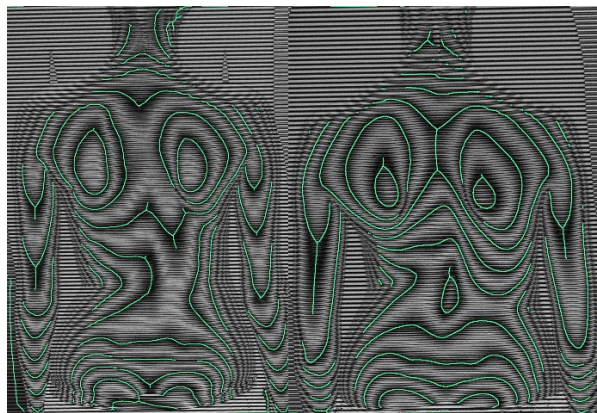


Figure 16
Segmented moiré fringes of image no. 3 (L) and 10 (R)

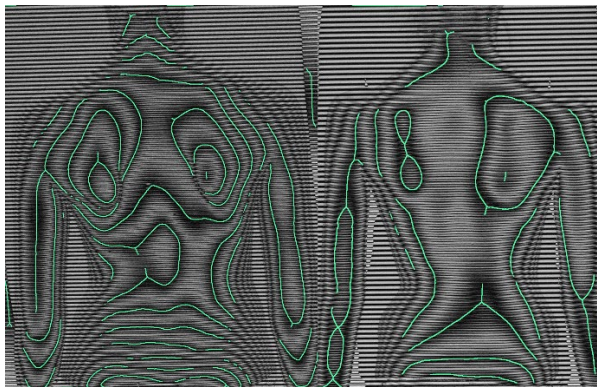


Figure 17
Segmented moiré fringes of image no. 5 (L) and 6 (R)

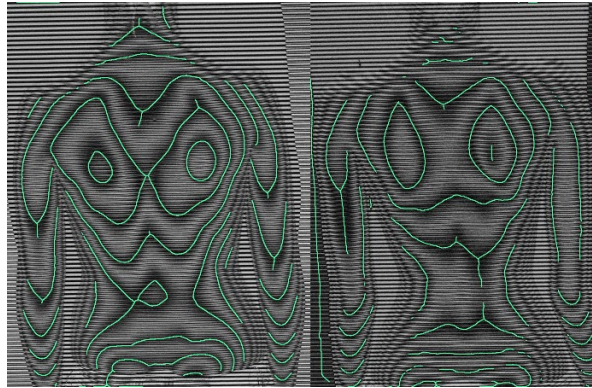


Figure 18
Segmented moiré fringes of image no. 7 (L) and 9 (R)

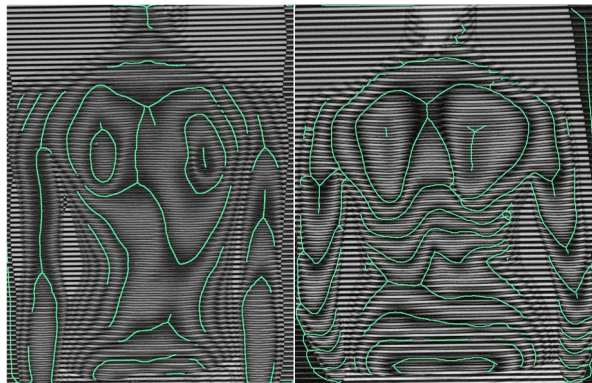


Figure 19
Segmented moiré fringes of image no. 4 (L) and 8 (R)

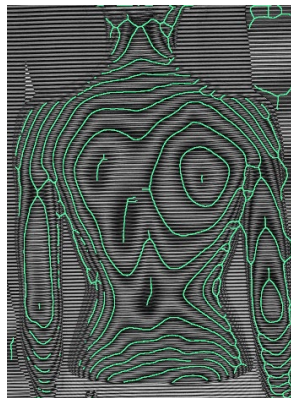


Figure 20
Segmented moiré fringes of image no. 11

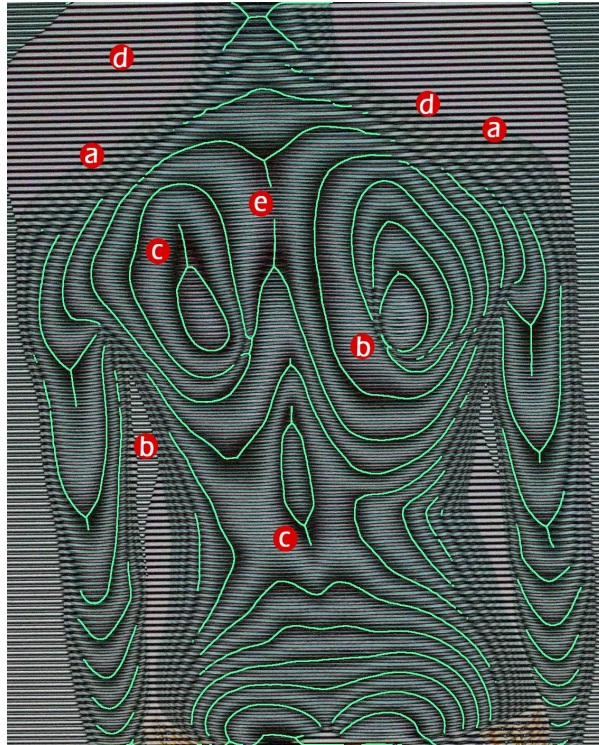


Figure 21

Problems to be handled in moiré fringe segmenting algorithm
(a-c) pale, convergent, and wider/blurred moiré fringes
(d) noise of residual grating
(e) unwanted branches

Conclusion

In this study, an initial phase of research on MF segmentation of scoliotic spines is conducted, presenting an algorithmic sequence of filtering and morphological operations with static function parameters in MATLAB® environment. The applicability of the algorithm is confirmed by a simple, fast to process and, for the most part of sample images, accurate MF segmentation. The results indicate that the algorithm introduced constitutes a suitable base for further research on segmenting MFs with adaptive and dynamic function parameters and adaptive image processing solutions and replacing time demanding and complex image processing techniques.

Acknowledgment

We would like to express our gratitude to Salus Orthopedtechnika Kft. (István Joó, Katalin Prommer, Ferenc Marlok) for providing us sample images and granting permission to our study.

References

- [1] J. W. S. Rayleigh. On the manufacture and theory of diffraction gratings. *Philosophical Magazine*, 47:81-93, 1874
- [2] H. Takasaki. Moiré topography. *Applied Optics*, 9(6):1467-72, 1970
- [3] H. Takasaki. Moiré topography. *Applied Optics*, 12(4):845-52, 1973
- [4] Takei T., Yokosawa S., Innami T., Miyazawa T., Kuwana T., Takagi M., Furukawa A. Application of Moiré Topography to Forensic Odontology. *The Journal of Nihon University School of Dentistry*, Vol. 27(2), 1985, 87-104
- [5] Wood, J. D.; Wang, R.; Weiner, S.; Pashley, D. H. Mapping of tooth deformation caused by moisture change using moiré interferometry. *Dent. Mater.*, Vol. 19(3), 2003, 159-166
- [6] Jelen K., Kusová S. Pregnant women: Moiré contourgraph and its semiautomatic and automatic evaluation. Dedicated to Professor Antonín Dolezal on his 75th birthday anniversary. *Neuro endocrinology letters*, Vol. 25, 2004, 52-56
- [7] Á. Antal. Optikai úton generált Moiréfelületek hibaanalízise és identifikálása mérés technikai alkalmazásokkal [dissertation on the internet]. Budapest, Hungary, University of Technology and Economics, 2009 [cited 2021 February 24] Available from: <https://repozitorium.omikk.bme.hu/bitstream/handle/10890/851/ertekezes.pdf?sequence=1&isAllowed=y>
- [8] F. Porto, J. L. Gurgel, T. Russomano, P. T. V. Farinatti. Moiré Topography: From Takasaki Till Present Day. In Grivas T. B., Editor: *Recent advances in scoliosis*, pp. 103-118, 2012
- [9] M. Batouche, R. Benlamri. A computer vision system for diagnosing scoliosis. In *Proceedings of IEEE International Conference on Systems, Man and Cybernetics*, 3, pp. 2623-2628, 1994
- [10] H. S. Kim, S. Ishikawa, Y. Ohtsuka, H. Shimizu, T. Shinomiya, M. A. Viergever. Automatic scoliosis detection based on local centroids evaluation on Moiré topographic images of human backs. *IEEE Trans Med Imaging*, 20(12):1314-1320, 2001
- [11] T. Ikeda, H. Terada. Development of the moiré method with special reference to its application to biostereometrics. *Opt. Laser Technol.*, 12:302-306, 1981
- [12] H. Kim, H. Ushijima, S. Ishikawa, Y. Otsuka, H. Shimizu, T. Shinomiya, M. A. Viergever. Scoliosis detection based on difference of apexes position and angle on Moiré topographic images. *International Congress Series*, 1268:1294, 2004

- [13] P. Balla, G. Manhertz, Á. Antal. Diagnostic moiré image evaluation in spinal deformities. *Optica Applicata*, 46:375-385, 2016
- [14] H. Zhi, R. B. Johansson. Interpretation and classification of fringe patterns. *Optics and Lasers in Engineering*, 17(1):9-25, 1992
- [15] MATLAB (2018) 9.5.0.944444 (R2018b). Natick, Massachusetts: The MathWorks Inc.
- [16] H. W. Wing, Y. S. Kin. Moiré Fringe Segmentation Using Fuzzy Inference System. In: H. Ibrahim, S. Iqbal, S. S. Teoh, M. T. Mustaffa, Editors: *9th International Conference on Robotic, Vision, Signal Processing and Power Applications*. Lecture Notes in Electrical Engineering, 398. Springer, Singapore, 2017